Electronic Supplementary Material (ESI)

Toward improving the photocatalytic activity of $BiVO_4$–graphene 2D–2D composites under visible light by the addition of mediator

Zi-Rong Tang,*[a] Qianqian Yu,[a] and Yi-Jun Xu[a,b]

[a] *College of Chemistry, New Campus, Fuzhou University, Fuzhou, 350108, P.R. China.*
[b] *State Key Laboratory of Photocatalysis on Energy and Environment, College of Chemistry, Fuzhou University, Fuzhou, 350002, P.R. China.*
**To whom correspondence should be addressed. Tel. /fax: +86 591 22866126*
E-mail Address: zrtang@fzu.edu.cn

Contents list

Experimental section

Preparation

Materials. Ammonium metavanadate (NH_4VO_3), bismuth (III) nitrate pentahydrate ($Bi(NO_3)_3{\cdot}5H_2O$), sodium dodecylbenzenesulfonate ($C_{18}H_{29}NaO_3S$), sodium hydroxide (NaOH), palladium chloride ($PdCl_2$), sulfuric acid (H_2SO_4), nitric acid (HNO_3), graphite powder, hydrochloric acid (HCl), phosphorus pentoxide (P_2O_5), potassium persulfate ($K_2S_2O_8$), potassium permanganate ($KMnO_4$), hydrogen peroxide, 30% (H_2O_2), N,N-Dimethylflormamide (C_3H_7NO) and ethanol (C_2H_6O) were obtained from Sinopharm Chemical Reagent Co., Ltd. (Shanghai, China). All materials were used as received without further purification. Deionized (DI) water used in the synthesis was from local sources.

Synthesis. *(I) Synthesis of Graphene Oxide*. GO was firstly synthesized from natural graphite powder by a modified Hummers method.[1-3] *(II) Fabrication of $BiVO_4$ Nanosheets.* The protocol of preparing $BiVO_4$ nanosheets is as the following.[4] Briefly, 1.0 mmol of $Bi(NO_3)_3{\cdot}5H_2O$ and 0.72 mmol of $C_{18}H_{29}NaO_3S$ (SDBS) were initially dissolved in 10.0 mL of 4.0 M HNO_3 solution and the resultant solution was marked as A solution. Simultaneously, 1.0 mmol of NH_4VO_3 was added to 10.0 mL of 2.0 M NaOH solution, and the resultant solution was marked as B solution. Then, B solution was added into the A solution drop by drop under vigorous stirring. After 0.5 h, the pH value of the mixed solution was adjusted to 6.5 with 2.0 M NaOH solution. After 0.5 h, the resultant solution was sealed in a 50 mL Teflon-lined stainless steel autoclave. The autoclave was heated to 160 °C and maintained for 60 min, and then allowed to cool to room temperature. The vivid yellow precipitate was collected after centrifugation, washed with deionized water and absolute alcohol, and then dried at 100 °C for 4 h. *(III) Synthesis of $BiVO_4$ Nanosheets–GR Composites.* The $BiVO_4$ nanosheets–GR composites were synthesized by a simple hydrothermal reaction. GO was ultrasonicated in 100 mL of deionized water to disperse it well. After that, 0.2 g of $BiVO_4$ nanosheets was added to the calculated amount of the above GO solution to prepare a series of $BiVO_4$ nanosheets–GR composites with different weight addition ratios of GR to $BiVO_4$ nanosheets. The mixture was continued to be ultrasonicated for 5 min to obtain a homogeneous suspension and then it was stirred vigorously with the formation of light green floc. After being washed with DI water, this light green floc was dispersed in 80 mL of DI water and transferred into a 100 mL Teflon-sealed autoclave and maintained at 120 °C for 12 h. The dark green precipitates were collected after centrifugation, washed thoroughly with DI water and ethanol, and then fully dried in oven at 60 °C. Ultimately, a series of $BiVO_4$ nanosheets–GR composites with different weight addition ratios of GR were obtained. *(Ⅳ) Synthesis of Pd–PRGO (partially reduced graphene oxide).* The protocol of preparing Pd-PRGO was modified from the previously reported method.[5] In detail, 208.7 μL of 10 mM H_2PdCl_4 aqueous solution was added into a certain volume of 1 $mg{\cdot}mL^{-1}$ of GO aqueous solution and the mixture was kept stirring for 30 min in an ice bath. When the reaction was finished, the as-obtained Pd-PRGO was recovered by suction filtration using the Buchner funnel and washed with DI water sufficiently. Then, the Pd-PRGO on the filter paper was dispersed in the 80 mL of DI water. *(Ⅴ) Synthesis of $BiVO_4$ Nanosheets–GR–Pd Composites.* 0.2 g of $BiVO_4$ nanosheets was added to the calculated amount of the above 100 mL of PRGO–Pd aqueous solution to prepare a series of $BiVO_4$ nanosheets–GR–Pd composites with different weight addition ratios of GR to $BiVO_4$ nanosheets. The following steps of preparing $BiVO_4$ nanosheets–GR–Pd composites are the same as that of $BiVO_4$ nanosheets–GR composites as described above. *(Ⅵ) Synthesis of $BiVO_4$ Nanosheets–Pd Composite.* The $BiVO_4$–Pd

nanocomposite was prepared *via* a two-step method. Firstly, 10 mL of 2.0 mM H_2PdCl_4 solution, 30 mL of H_2O and 0.0889 g of PVP (average molecular weight of PVP 40 000) was mixed homogeneously. Then, 2.4 mL of 0.1 M $NaBH_4$ aqueous solution was added to the above solution quickly; after that, the mixture was stirred for 5 h and the resulting Pd colloids was obtained. In a following step, the synthesis of $BiVO_4$–Pd was done as following: 2.2 mL of the prepared Pd colloids was added to 50 mL of $BiVO_4$ suspension (0.1 g) to prepare the $BiVO_4$–0.11% Pd composite (equivalent to the weight ratio of Pd in the optimal $BiVO_4$ nanosheets–2% GR–Pd photocatalyst). The mixing solution was aged with vigorous stirring for 2 h to obtain a homogeneous suspension. Then, this suspension was evaporated in a rotary evaporator in vacuum in a water bath at 323 K and then fully dried at 393 K in an oven.

Characterization

X-ray powder diffraction (XRD) patterns of the samples were recorded on a Philip X' Pert Pro MPP X-ray diffractometer (XRD) at 40 kV and 40 mA in the 2θ ranging from 10° to 80° with a scan rate of 5° per minute. Raman spectroscopic measurements were performed on a Renishaw in Via Raman System 1000 with a 532 nm Nd:YAG excitation source at room temperature. X-ray photoelectron spectroscopy (XPS) measurements were carried out on a Thermo Scientific ESCA Lab250 spectrometer which consists of a monochromatic Al Kα as the X-ray source, a hemispherical analyzer and sample stage with multiaxial adjustability to obtain the surface composition of the sample. The optical properties of the samples were characterized by the UV-vis diffuse reflectance spectroscopy (DRS) using a on a Cary−500 UV-vis-NIR spectrometer over a wavelength range of 200-800 nm, during which $BaSO_4$ was employed as the internal reflectance standard. Transmission electron microscopy (TEM) images and high-resolution transmission electron microscopy (HRTEM) images were obtained using a FEI F2 instrument at an accelerating voltage of 200 kV. The photoluminescence (PL) spectra were obtained using an Edinburgh FL-FS 920 TCSPC system with an excitation wavelength of 420 nm.

The electrochemical analysis was carried out in a conventional three electrode cell using a Pt electrode and an Ag/AgCl electrode as the counter electrode and reference electrode, respectively. The working electrode was prepared on fluorine-doped tin oxide (FTO) conductor glass. In detail, the sample powder (5 mg) was ultrasonicated in 0.5 mL N, N-Dimethylflormamide (DMF) to disperse it evenly to get slurry. The slurry was spreading onto FTO glass, whose side part was previously protected using scotch tape. The working electrode was dried overnight under ambient conditions. A copper wire was connected to the side part of the working electrode using conductive tape. Uncoated parts of the electrode were isolated with epoxy resin. The transient photocurrent was measured with a home-made three electrode quartz cell with a PAR VMP3 Multi Potentiostat apparatus and the electrolyte was 0.2 M aqueous Na_2SO_4 solution (pH = 6.8) without additive. The visible light irradiation source was a 300W Xe arc lamp system equipped with a UV−CUT filter (λ>420 nm). The Nyquist impedance was measured with a CHI-660D electrochemical workstation (CH instruments, USA) and the electrolyte consisted of 0.01 M potassium hexacyanoferrate (III), 0.01 M Potassium hexacyanoferrate (II) and 0.5 M KCl.

Photocatalytic activity

In a typical photocatalytic reaction, a 300 W Xe arc lamp (PLS-SXE 300, Beijing Perfect light Co., Ltd.) with a UV−CUT filter to cut off light of wavelength λ < 420 nm was used as the

irradiation source. Rhodamine B (RhB) and methyl orange (MO) were used as model dye molecules to assay the photocatalytic activity of $BiVO_4$ nanosheets–GR–Pd composites. The as-prepared $BiVO_4$ nanosheets–GR–Pd composites (20 mg) were dispersed into an aqueous solution of RhB (100ml, 10 $mg \cdot L^{-1}$) or an aqueous solution of MO (50 mL, 5 $mg \cdot L^{-1}$). Before visible light illumination, the above suspensions were stirred in the dark for 2 h to ensure the establishment of adsorption−desorption equilibrium between the samples and reactants. During the reaction process, 4 mL of sample solution was collected at a certain time interval and centrifuged at 10000 rpm for 10 min to remove the catalyst completely. The dye concentration of the supernatant was analyzed on an ultraviolet-visible light spectrophotometer (Lambda UV-1750).

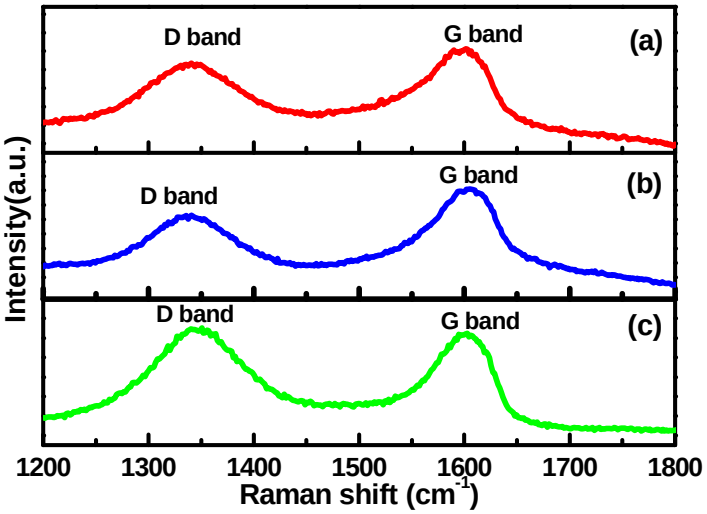

Fig. S1 Raman spectra of $BiVO_4$ nanosheets–2% GR–Pd composite (a), $BiVO_4$ nanosheets–1% GR composite (b) and GO (c).

Note: It can be seen from **Fig. S1** that all of GO, $BiVO_4$ nanosheets–1% GR composite and $BiVO_4$ nanosheets–2% GR–Pd composite exhibit Raman shifts at about 1600 and 1345cm^{-1}, corresponding to the D-band and G-bands, respectively. Generally, the D band is a breathing mode of κ-point phonons of A1g symmetry, while the G band is usually assigned to the E_{2g} phonon of C sp^2 atoms.[6] Of particular note is the intensity ratio of the D band (~1345 cm^{-1}) and G band (~1600 cm^{-1}), I_D/I_G, which is a measure of the relative concentration of local defects or disorders (particularly the sp^3-hybridized defects) compared to the sp^2-hybridized GR domains.[7-9] We can see from Fig. S1 that the I_D/I_G ratio is 1.04 for GO. After the hydrothermal reaction, the I_D/I_G ratios for $BiVO_4$ nanosheets–1% GR composite and $BiVO_4$ nanosheets–2% GR–Pd composite are 0.83 and 0.89, respectively, indicating their more graphitization than that of GO.

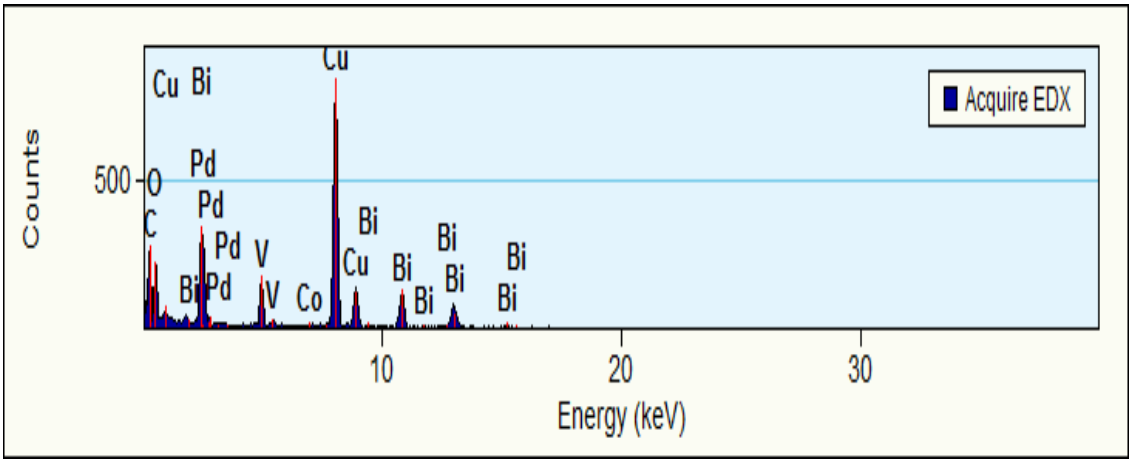

Fig. S2 EDX of $BiVO_4$ nanosheets–2% GR–Pd composite.

Note: The EDX spectra clearly evidence the presence of elements Pd, Bi, V, O and C for the as-synthesized $BiVO_4$ nanosheets–2% GR–Pd composite.

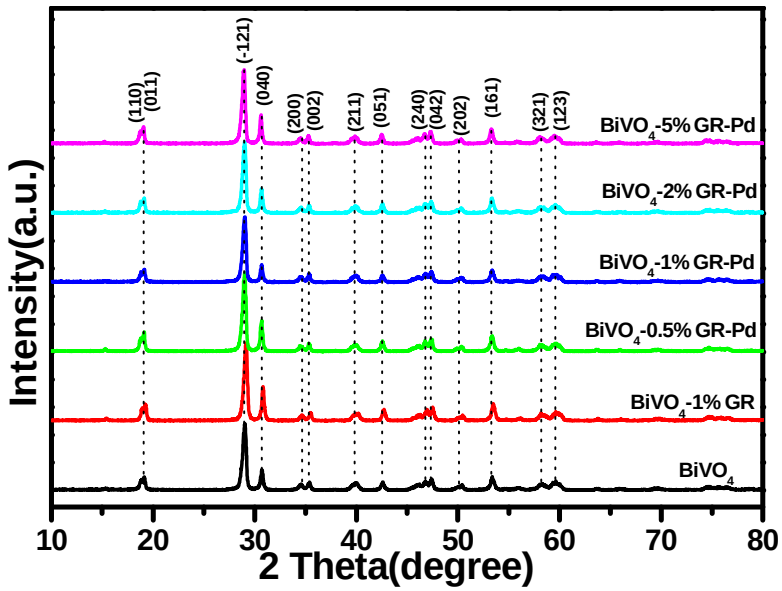

Fig. S3 The XRD patterns of $BiVO_4$ nanosheets, $BiVO_4$ nanosheets–1% GR composite and $BiVO_4$ nanosheets–GR–Pd composites with different weight addition ratios of GR.

Note: Fig S3 shows the XRD spectra of $BiVO_4$ nanosheets, $BiVO_4$ nanosheets–1% GR and ternary $BiVO_4$ nanosheets–GR–Pd composites with different weight addition ratios of GR. The $BiVO_4$ nanosheets–GR–Pd composites exhibit similar XRD patterns to the $BiVO_4$ nanosheets and binary $BiVO_4$ nanosheets–1% GR. The main peaks at 2θ values of 18.7, 19.0, 28.8, 30.5, 34.5, 35.2, 39.8, 42.5, 46.7, 47.3, 50.3, 53.3, 58.5 and 59.3° can be indexed to (110), (011), (-121), (040), (200), (002), (211), (051), (240), (042), (202), (161), (321) and (123) crystal planes, respectively, which can be assigned to the monoclinic $BiVO_4$ (JCPDS No. 14-0688).

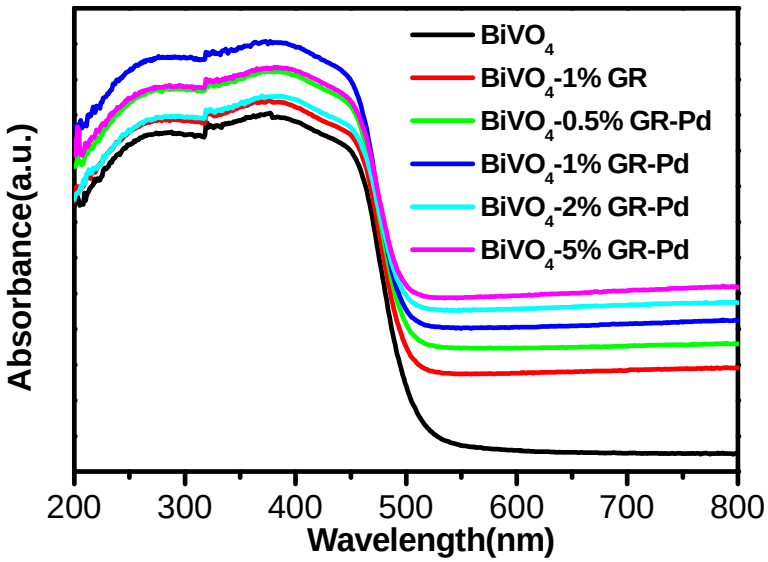

Fig. S4 UV-visible diffuse reflectance spectra (DRS) of $BiVO_4$ nanosheets, $BiVO_4$ nanosheets–1% GR composite and $BiVO_4$ nanosheets–GR–Pd composites with different weight addition ratios of GR.

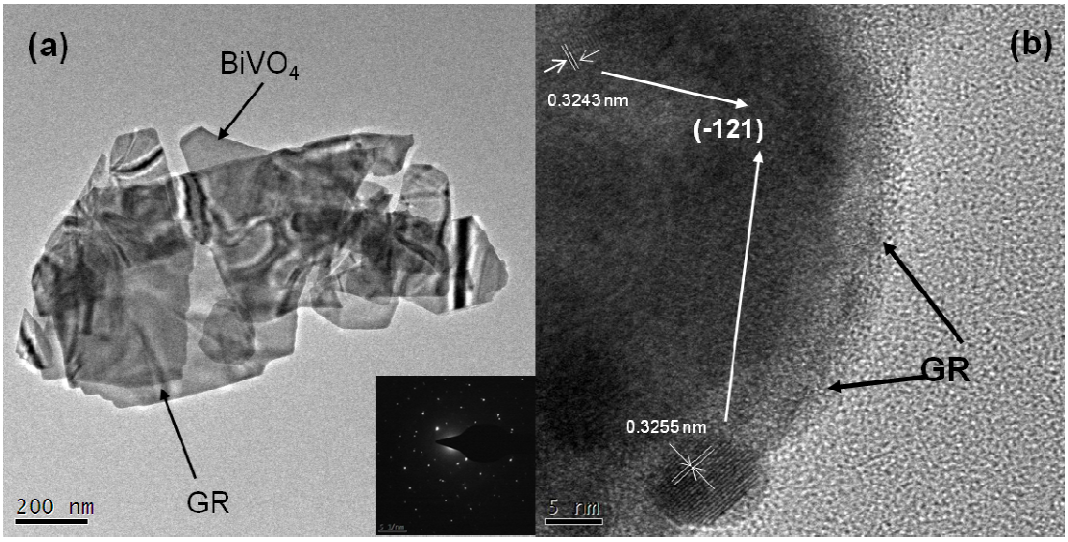

Fig. S5. TEM (a) and HRTEM (b) images for the $BiVO_4$ nanosheets–1% GR composite; the inset of (a) is the image of the SAED pattern.

Note: As can be seen from the TEM analysis in **Fig. S5 (a)**, the GR sheets have a good interfacial contact with $BiVO_4$ nanosheets, and there is an overlap between $BiVO_4$ nanosheets and GR sheets. The selected area electron diffraction (SAED) in **Fig. S5 (a)** pattern indicates that the $BiVO_4$ nanosheets–1% GR composite possesses single-crystal structure. The high-resolution TEM (HRTEM) image in **Fig. S5 (b)** shows that the spacing of lattice fringe is measured to be 0.325 nm, corresponding to the (-121) crystal plane of monoclinic $BiVO_4$, which is also in accordance with the result of XRD analysis in **Fig. S3**.

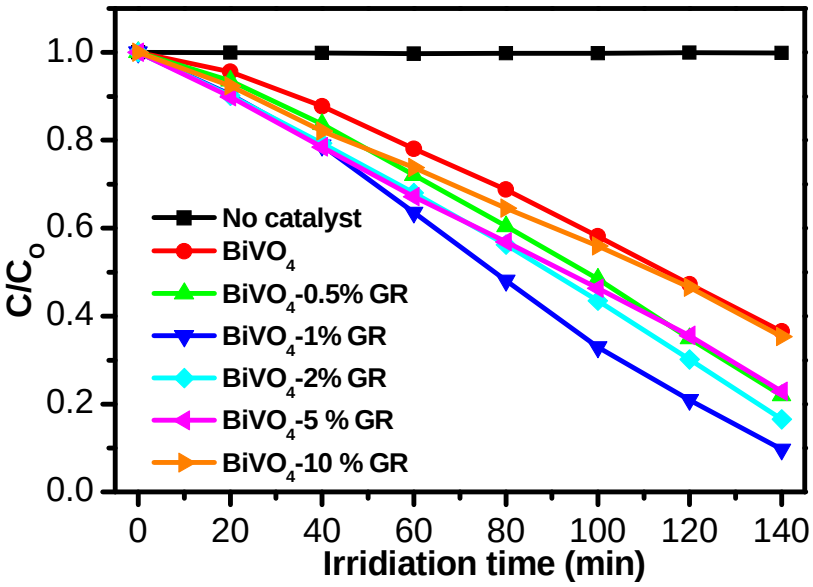

Fig. S6. Time-online photocatalytic performance of $BiVO_4$ nanosheets and $BiVO_4$ nanosheets–GR composites with different weight addition ratios of GR for the degradation of Rhodamine B (RhB) under visible light irradiation ($\lambda > 420$ nm).

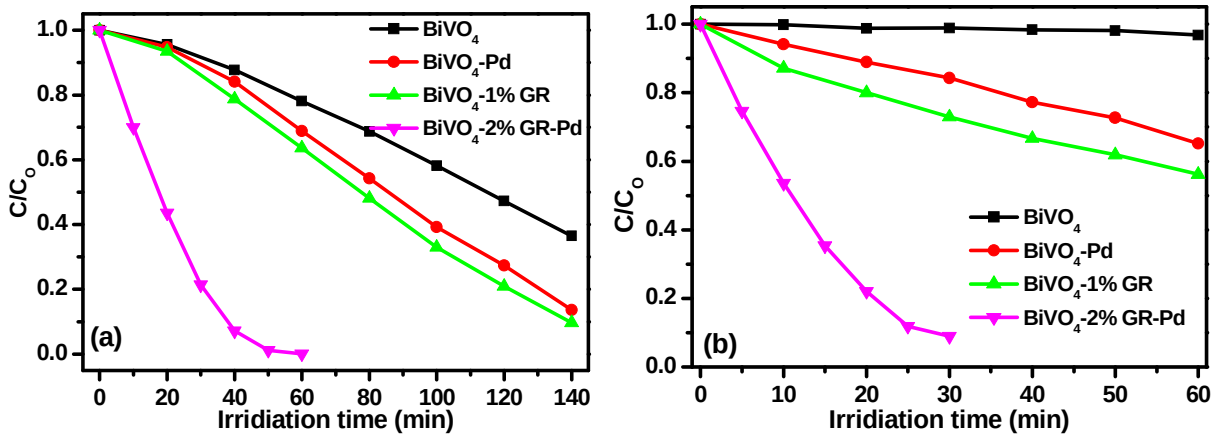

Fig. S7 Time-online photocatalytic performance of degradation of Rhodamine B (a) and methyl orange (b) under visible light irradiation ($\lambda > 420$ nm) over blank $BiVO_4$ nanosheet, $BiVO_4$ nanosheets–Pd, $BiVO_4$ nanosheets–1% GR and $BiVO_4$ nanosheets–GR–Pd composite.

Note: The weight ratio of Pd in $BiVO_4$ nanosheets–Pd is the same as that in $BiVO_4$ nanosheets–GR–Pd composite.

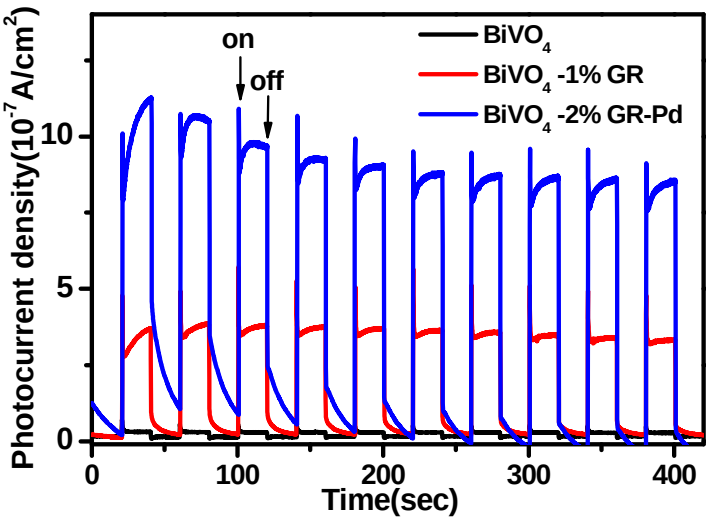

Fig. S8 Transient photocurrent density of $BiVO_4$ nanosheets, $BiVO_4$ nanosheets–1% GR composite and $BiVO_4$ nanosheets–2% GR–Pd composite in 0.2 M Na_2SO_4 aqueous solution (pH =6.8) without bias versus Ag/AgCl (0 V *vs.* Ag/AgCl) under the irradiation of visible light ($\lambda > 420$ nm).

Note: As shown in **Fig. S8**, $BiVO_4$ nanosheets–2% GR–Pd composite shows significantly enhanced photocurrent density as compared with $BiVO_4$ nanosheets–1% GR composite. Because the photocurrent is formed mainly by the diffusion of the photogenerated electrons to the back contact, and meanwhile the photogenerated holes are taken up by the hole acceptor in the electrolyte,[3, 10] the enhanced photocurrent density over $BiVO_4$ nanosheets–2% GR–Pd composite indicates a more efficient separation of the photoexcited electron–hole pairs and a longer lifetime of the photogenerated charge carriers than $BiVO_4$ nanosheets–1% GR composite.

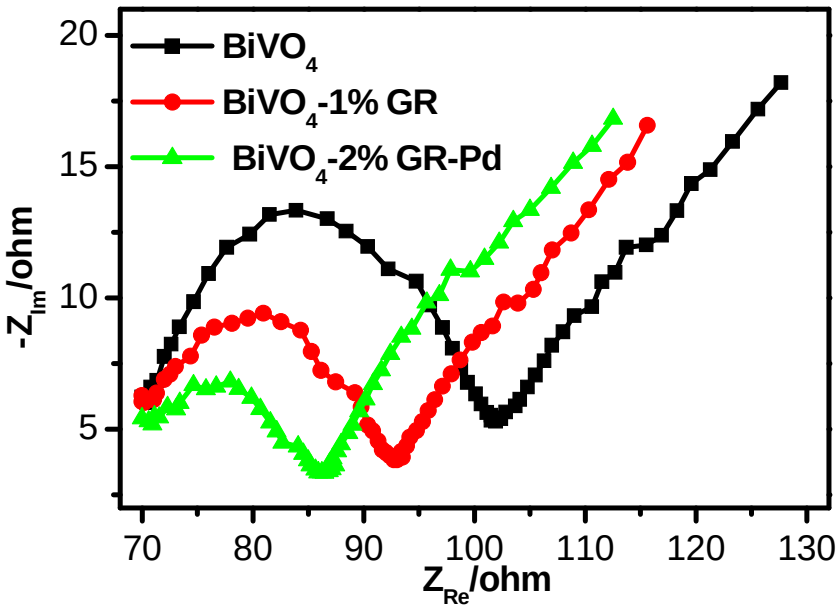

Fig. S9 Nyquist impedance plots of $BiVO_4$ nanosheets, $BiVO_4$ nanosheets–1% GR composite and $BiVO_4$ nanosheets–2% GR–Pd composite performed under the potential of 0.29 V (the value of open circuit voltage).

Note: Fig. S9 shows the electrochemical impedance spectroscopy (EIS) Nyquist plots of $BiVO_4$ nanosheets, $BiVO_4$ nanosheets–1% GR composite and $BiVO_4$ nanosheets–2% GR–Pd composite, all of which show depressed semicircles at high frequencies. Since the preparation method of electrodes and the electrolyte used is the same, the high frequency semicircle is related to the resistance of electrodes and the slope of the EIS Nyquist plots in the low frequency range is due to diffusion of redox species in the elecctrolyte.[11] In electrochemical spectra, the high-frequency arc corresponds to the charge transfer limiting process, which can be attributed to the double-layer capacitance (C_{dl}) in parallel with the charge transfer resistance (R_{ct}) at the contact interface between electrode and electrolyte solution.[12, 13] $BiVO_4$ nanosheets–2% GR–Pd composite has a smallest arc as compared to $BiVO_4$ nanosheets and $BiVO_4$ nanosheets–1% GR composite, thus suggesting the more efficient interfacial charge transfer over $BiVO_4$ nanosheets–2% GR–Pd composite than that of $BiVO_4$ nanosheets and $BiVO_4$ nanosheets–1% GR composite.

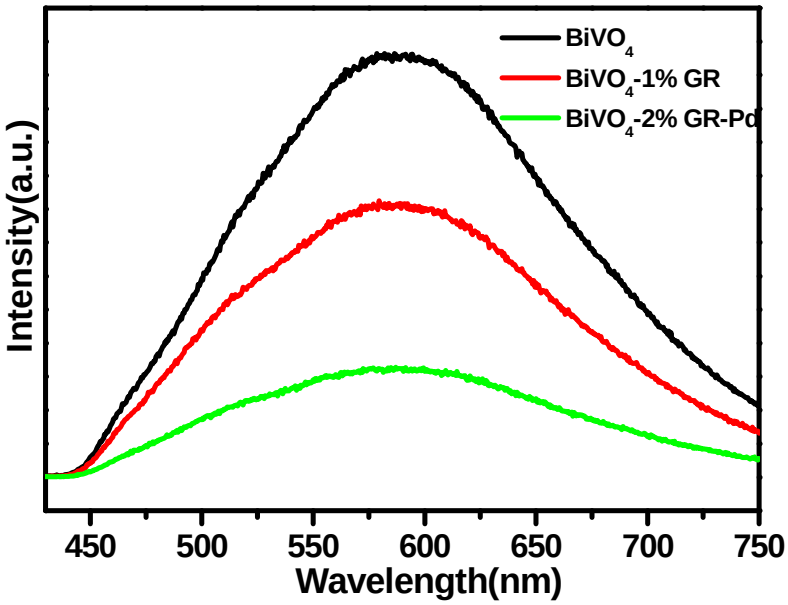

Fig. S10 Photoluminescence spectra of $BiVO_4$ nanosheets, $BiVO_4$ nanosheets–1% GR composite and $BiVO_4$ nanosheets–2% GR–Pd composite with an excitation wavelength of 420 nm.

Note: Photoluminescence (PL) spectra are able to reflect the fate and transfer of photogenerated charge carriers that in principle are the most key factors determining the overall photoactivity of semiconductor-based materials.[14, 15] On the basis of PL data as displayed in **Fig. S10**, under an excitation wavelength of 420 nm, the PL emission wavelength of all samples is centered at 590 nm, which is attributed to the recombination of holes in the valence band and electrons in the conduction band. The PL intensity obtained over $BiVO_4$ nanosheets–2% GR–Pd composite is much weaker than that of $BiVO_4$ and $BiVO_4$–1% GR composite, thus suggesting the longer lifetime of photogenerated charge carriers from $BiVO_4$ nanosheets–2% GR–Pd composite.

Reference

1. W. S. Hummers Jr and R. E. Offeman, *J. Am. Chem. Soc.*, 1958, **80**, 1339-1339.
2. Y. Zhang, Z.-R. Tang, X. Fu and Y.-J. Xu, *ACS Nano*, 2010, **4**, 7303-7314.
3. N. Zhang, Y. Zhang, X. Pan, X. Fu, S. Liu and Y.-J. Xu, *J. Phys. Chem. C*, 2011, **115**, 23501-23511.
4. a) L. Zhang, D. R. Chen and X. L. Jiao, *J. Phys. Chem. B*, 2006, **110**, 2668-2673. b) Q. Yu, Z.-R. Tang and Y.-J. Xu, *J. Energ. Chem.*, 2014, **23**, 564-574.
5. X. Chen, G. Wu, J. Chen, X. Chen, Z. Xie and X. Wang, *J. Am. Chem. Soc.*, 2011, **133,** 3693–3695.
6. E. Gao, W. Wang, M. Shang and J. Xu, *Phys. Chem. Chem. Phys.*, 2011, **13**, 2887-2893.
7. Y. Yan, S. Sun, Y. Song, X. Yan, W. Guan, X. Liu and W. Shi, *J. Hazard. Mater.*, 2013, **250-251**, 106-114.
8. S. Chen, J. Zhu and X. Wang, *J. Phys. Chem. C*, 2010, **114**, 11829-11834.
9. S. Stankovich, D. A. Dikin, R. D. Piner, K. A. Kohlhaas, A. Kleinhammes, Y. Jia, Y. Wu, S. T. Nguyen and R. S. Ruoff, *Carbon*, 2007, **45**, 1558-1565.
10. Z. Chen, S. Liu, M.-Q. Yang and Y.-J. Xu, *ACS Appl. Mater. Interfaces*, 2013, **5**, 4309-4319.

11. L. Gao, X. Wang, Z. Xie, W. Song, L. Wang, X. Wu, F. Qu, D. Chen and G. Shen, *J. Mater. Chem. A*, 2013, **1**, 7167-7173.
12. H.-L. Guo, X.-F. Wang, Q.-Y. Qian, F.-B. Wang and X.-H. Xia, *ACS Nano*, 2009, **3**, 2653-2659.
13. T. Lu, Y. Zhang, H. Li, L. Pan, Y. Li and Z. Sun, *Electrochim. Acta*, 2010, **55**, 4170-4173.
14. Y. Zhang, N. Zhang, Z.-R. Tang and Y.-J. Xu, *ACS Nano*, 2012, **6**, 9777-9789.
15. Y. Zhang, N. Zhang, Z.-R. Tang and Y.-J. Xu, *Phys. Chem. Chem. Phys.*, 2012, **14**, 9167-9175.